

## Photoacoustic characterization of carbon nanotube array thermal interfaces

Baratunde A. Cola, Jun Xu, Changrui Cheng, Xianfan Xu, and Timothy S. Fisher<sup>a)</sup>

*School of Mechanical Engineering, Purdue University, West Lafayette, Indiana 47907,  
and Birc Nanotechnology Center, Purdue University, West Lafayette, Indiana 47907*

Hanping Hu

*Department of Thermal Science and Energy Engineering, University of Science and Technology of China,  
Hefei, Anhui, China*

(Received 23 June 2006; accepted 17 December 2006; published online 12 March 2007)

This work describes an experimental study of thermal conductance across multiwalled carbon nanotube (CNT) array interfaces, one sided (Si-CNT-Ag) and two sided (Si-CNT-CNT-Cu), using a photoacoustic technique (PA). Well-anchored, dense, and vertically oriented multiwalled CNT arrays have been directly synthesized on Si wafers and pure Cu sheets using plasma-enhanced chemical vapor deposition. With the PA technique, the small interface resistances of the highly conductive CNT interfaces can be measured with accuracy and precision. In addition, the PA technique can resolve the one-sided CNT interface component resistances (Si-CNT and CNT-Ag) and the two-sided CNT interface component resistances (Si-CNT, CNT-CNT, and CNT-Cu) and can estimate the thermal diffusivity of the CNT layers. The thermal contact resistances of the one- and two-sided CNT interfaces measured using the PA technique are  $15.8 \pm 0.9$  and  $4.0 \pm 0.4$  mm<sup>2</sup> K/W, respectively, at moderate pressure. These results compare favorably with those obtained using a steady state, one-dimensional reference bar method; however, the uncertainty range is much narrower. The one-sided CNT thermal interface resistance is dominated by the resistance between the free CNT array tips and their opposing substrate (CNT-Ag), which is measured to be  $14.0 \pm 0.9$  mm<sup>2</sup> K/W. The two-sided CNT thermal interface resistance is dominated by the resistance between the free tips of the mating CNT arrays (CNT-CNT), which is estimated to be  $2.1 \pm 0.4$  mm<sup>2</sup> K/W. © 2007 American Institute of Physics. [DOI: 10.1063/1.2510998]

### I. INTRODUCTION

Iijima<sup>1</sup> introduced carbon nanotubes (CNTs) to the greater scientific community in 1991, and CNTs have since gained much interest due to their outstanding physical and electrical properties that make them candidates for numerous potential applications.<sup>2</sup> An application of current interest, partially motivated by the intrinsically high thermal conductivity<sup>3–6</sup> and elastic modulus<sup>7,8</sup> of CNTs, is the use of CNT and carbon nanofiber (CNF) arrays synthesized directly on substrates for thermal contact conductance enhancement (i.e., reduction in interface resistance).<sup>9–18</sup> The reliable enhancement of thermal contact conductance is an important step in managing the heating issues faced by the semiconductor industry caused by increases in device and component densities. The 2005 International Technology Roadmap for Semiconductors<sup>19</sup> (ITRS) forecasts that by 2020 power dissipation levels of “cost-performance” and “high-performance” single-chip devices will be approximately 1 W/mm<sup>2</sup>. The ITRS identifies the need for thermal interface materials (TIMs) with increased thermal conductivity, improved adhesion, and higher elastic modulus. The extraordinary properties of CNTs plus the reported adhesive

behavior<sup>20</sup> of CNT array interfaces make them an excellent candidate material to meet the TIM needs detailed in the ITRS.

The fabrication and thermal characterization of directly synthesized CNT and CNF array TIMs have been the focus of recent studies.<sup>9–18</sup> Ngo *et al.*<sup>11</sup> used electrodeposited Cu as a gap filler to enhance the stability and thermal conductance of CNF arrays and reported a thermal resistance of 25 mm<sup>2</sup> K/W under a pressure of 0.414 MPa for Si–Cu interfaces measured with a one-dimensional (1D) steady state, reference bar method. Xu and Fisher<sup>13</sup> reported a thermal resistance of 20 mm<sup>2</sup> K/W for one-sided CNT array interfaces (Si-CNT-Cu) tested at a similar pressure with a reference bar method. The same CNT arrays as in the work of Xu and Fisher<sup>13</sup> were tested using the  $3\omega$  method by Hu *et al.*<sup>10</sup> at low pressures in the temperature range of 295–325 K. The effective thermal conductivity of the CNT samples, including voids, ranged from 74 to 83 W/m K. Thermal resistances between the free CNT array tips and an experimental contact were 17 and 15 mm<sup>2</sup> K/W at pressures of 0.040 and 0.100 MPa, respectively. Xu and Fisher<sup>14</sup> also combined thin layers of phase change material (PCM) with CNT arrays, and the composite produced a resistance of 5 mm<sup>2</sup> K/W under moderate pressures for Si–Cu interfaces. Wang *et al.*<sup>16</sup> used a photothermal technique to measure the thermal resistance between a CNT array and its growth substrate (Si-CNT). The resistance was relatively large, 16 mm<sup>2</sup> K/W, as the CNT

<sup>a)</sup>Author to whom correspondence should be addressed; electronic mail: tsfisher@purdue.edu

array was of poor structural quality and no pressure was applied to the interface. Using a transient thermoreflectance technique, Tong *et al.*<sup>17</sup> measured a thermal resistance of  $18 \text{ mm}^2 \text{ K/W}$  for a one-sided CNT interface (Si-CNT-glass). Tong *et al.*<sup>17</sup> also reported component resistances of the one-sided CNT interface (Si-CNT and CNT-glass). They concluded that the interface between the free CNT array tips and their opposing glass substrate (CNT-glass) dominated the total thermal interface resistance and suggested that this resistance could be further decreased by the application of pressure to the interface.

To achieve a dry, highly conductive thermal interface comparable to a soldered interface<sup>21</sup> ( $5 \text{ mm}^2 \text{ K/W}$ ), Xu and Fisher<sup>15</sup> fabricated and experimentally studied two-sided CNT interfaces with CNT arrays directly synthesized on Si wafers and Cu blocks. With well anchored and vertically oriented CNT arrays and using a reference bar method, an interface resistance less than  $5 \text{ mm}^2 \text{ K/W}$  for two-sided CNT interfaces was measured. However, due to CNT array fabrication constraints (e.g., difficulties in fabricating samples with identical CNT arrays on both sides of a test chip), a calibration experiment was necessary for their CNT interface reference bar measurements. The addition of this control experiment greatly increased measurement uncertainty, such that the uncertainty was larger than the magnitude of resistance.

The measurement techniques that have been used in prior work to characterize CNT array interfaces have limitations which include one if not all of the following: the inability to measure resistances on the order of  $1 \text{ mm}^2 \text{ K/W}$  or less precisely, the inability to individually resolve all the constitutive components of the total CNT interface resistance, and the inability to easily control the interface pressure during measurement. To facilitate further research on CNT array interface performance, a different measurement technique that can overcome these limitations is needed.

In photoacoustic (PA) measurements, a heating source (normally a laser beam) is periodically irradiated on a sample surface. The acoustic response of the gas above the sample is measured and related to the thermal properties of the sample. The PA phenomenon was explained by Rosencwaig and Gersho,<sup>22</sup> and an analytic solution of the PA response of a single layer on a substrate was developed. A more general analytic solution derived by Hu *et al.*<sup>23</sup> that explains the PA effect in multilayered materials is used in this study. A review of the PA technique was given by Tam,<sup>24</sup> and the technique has been used successfully to obtain the thermal conductivity of thin films.<sup>23,25–29</sup> The PA technique has also been used to measure the resistance of atomically bonded interfaces,<sup>23,28,29</sup> for which resistances were orders of magnitude less than the resistances measured in this study. The use of the PA technique for the measurement of thermal resistance of separable (nonbonded) interfaces has not been found in the literature, nor has the use of the PA technique with a pressurized acoustic chamber and sample.

The improvement of TIMs to meet the needs detailed in the ITRS can allow integrated circuits to satisfy the tight thermal budgets needed to maintain acceptable reliability standards; and the purpose of this work is to characterize

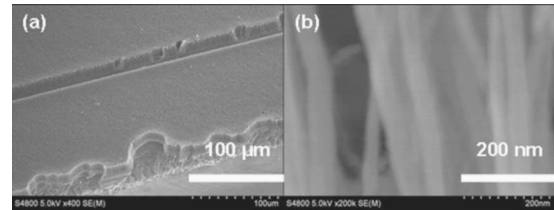


FIG. 1. SEM images of a CNT array synthesized on a Si substrate. (a) A  $30^\circ$ -tilted plane, top view of the vertically oriented and dense CNT array. The array height is estimated to be  $15 \mu\text{m}$ . The CNT array has a part across the top of the image that helps illustrate the uniformity of growth. (b) An image with higher magnification showing individual CNTs. CNT diameters range from 15 to 60 nm.

candidate interfaces that employ carbon nanotube arrays. In this work, a PA method is established to measure resistance values on the order of  $1 \text{ mm}^2 \text{ K/W}$ , to validate the results of measurement techniques with low precision, and to characterize resolved CNT thermal interface performance as a function of pressure. The room-temperature thermal interface resistance of a one-sided and a two-sided CNT interface at moderate pressures and their component resistances are measured using the PA method. The thermal diffusivity of each CNT array is estimated from PA measurements as well.

## II. SAMPLE FABRICATION AND EXPERIMENTAL SETUP

### A. CNT growth by plasma-enhanced chemical vapor deposition

All CNT array samples considered in this work were grown on Si (with roughness measures of  $R_a=0.01 \mu\text{m}$  and  $R_z=0.09 \mu\text{m}$ , calculated according to Ref. 30) and Cu ( $R_a=0.05 \mu\text{m}$  and  $R_z=0.5 \mu\text{m}$ , calculated according to Ref. 30) surfaces with a trilayer (Ti/Al/Ni) catalyst configuration<sup>14</sup> by direct synthesis with microwave plasma-enhanced chemical vapor deposition (PECVD)<sup>31–33</sup> employing  $\text{H}_2$  and  $\text{CH}_4$  feed gases. Si and Cu were chosen as growth substrates in order to arrange an interface which is representative of a common heat sink to chip assembly. Similar to the work of Xu and Fisher,<sup>14,15</sup> the thicknesses of Ti, Al, and Ni metal layers were 30, 10, and 6 nm, respectively. The working pressure of the PECVD chamber was 10 torr, the sample stage temperature was  $800^\circ\text{C}$ , and the microwave plasma power was 150 W. The volumetric flow rates of  $\text{H}_2$  and  $\text{CH}_4$  were 72 and 8 SCCM (SCCM denotes cubic centimeter per minute at STP), respectively, and the growth period was approximately 20 min. Figure 1(a) shows a  $30^\circ$ -tilted plane, top view of the CNT array synthesized on Si. The array height is approximately  $15 \mu\text{m}$ . CNT diameters for the array on the Si wafer range from 15 to 60 nm [Fig. 1(b)]. Figure 2 shows that, with identical catalyst preparation, the CNT array synthesized on the Cu sheet is very similar to the array on the Si wafer. The array height is approximately  $20 \mu\text{m}$  [Fig. 2(a)], and the CNT diameters also range from 15 to 60 nm [Fig. 2(b)]. A CNT array was grown on a Cu block, which protruded into the plasma and had sharp edges, in a prior study [inset of Fig. 2(a)].<sup>15</sup> The block acted like an antenna to concentrate the plasma energy around its corners and edges. This plasma concentration had a strong etching effect on the

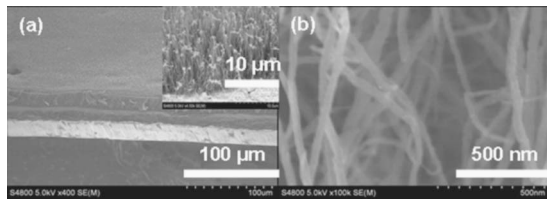


FIG. 2. SEM images of a CNT array synthesized on a pure Cu sheet. (a) Cross-section view of the vertically oriented and dense CNT array. The array height is estimated to be approximately 20  $\mu\text{m}$ ; the inset shows the CNT array grown on a 1 cm tall Cu bar from previous work (Ref. 15). (b) An image with higher magnification showing individual CNTs. The CNT diameters range from 15 to 60 nm.

CNT growth surface. By comparison, the height and density of the array on the Cu sheet are greatly improved because the plasma did not concentrate on the sheet during CNT growth. The CNT density of all arrays in this study, determined by counting CNTs in a representative area of a scanning electron microscope (SEM) image, was approximately  $6 \times 10^8$  CNTs/ $\text{mm}^2$ . Assuming an average CNT diameter of approximately 30 nm, an approximate CNT volume fraction of 42% can be calculated by assuming the CNTs are circular tubes of uniform height that are vertically aligned. Individual multiwalled CNTs are less porous than fullerenes; thus, they should possess a mass density between that of fullerenes, 1900  $\text{kg}/\text{m}^3$ ,<sup>34</sup> and graphite, 2210  $\text{kg}/\text{m}^3$ .<sup>35</sup> By assuming a multiwalled CNT mass density of approximately 2060  $\text{kg}/\text{m}^3$ , the effective mass density of all the CNT arrays (including effects of void space) in this work is estimated to be approximately 865  $\text{kg}/\text{m}^3$ .

## B. Photoacoustic technique

The PA technique has been most commonly used to measure the thermal conductivity of thin films; however, the technique is capable of measuring interface resistance in a suitable configuration. Compared to other techniques to measure thermal conductance across thin films and planar interfaces, the PA technique is relatively simple, yet it provides high accuracy.<sup>28</sup>

### 1. Theory

In accordance with the generalized theory of the PA effect in multilayer materials,<sup>23</sup> the sample in a PA measurement can consist of any arbitrary number of layers, a backing material (0) and  $N$  successive layers (1, 2, ...,  $N$ ), and is heated by a modulated laser beam with an intensity of  $1/2I_0[1+\cos(\omega t)]$ , where  $\omega$  is the laser frequency. Absorption of the laser beam is allowed in any layer and in more than one layer. An additional gas medium ( $N+1$ ) is in contact with the surface layer ( $N$ ). The backing material (0) and gas medium ( $N+1$ ) are assumed to be thermally thick. Schematics of the one- and two-sided CNT interface samples in this work, along with the labeling of layers used in the PA model when estimating the total or lumped CNT interface resistance and the labeling of layers used in the PA model when estimating the component interface resistances and the thermal diffusivity of the CNT array(s), are shown in Fig. 3.

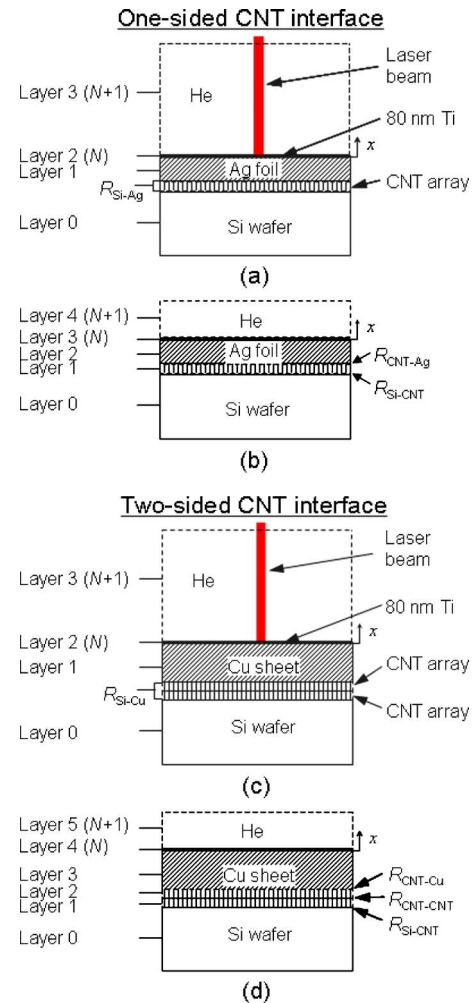


FIG. 3. (Color online) Schematic of the sample assemblies during PA measurement. (a) The CNT array is not considered a layer in the PA model, but rather as a contributor to the interface resistance between the Si wafer and the Ag foil,  $R_{\text{Si-Ag}}$ . (b) The CNT array is considered a layer in the PA model; therefore, the component resistances  $R_{\text{Si-CNT}}$  and  $R_{\text{CNT-Ag}}$  and the thermal diffusivity of the CNT array can be estimated. (c) The CNT arrays are not considered as layers in the PA model, but rather as contributors to the interface resistance between the Si wafer and the Cu sheet,  $R_{\text{Si-Cu}}$ . (d) The CNT arrays are considered as layers in the PA model; therefore, the component resistances  $R_{\text{Si-CNT}}$ ,  $R_{\text{CNT-CNT}}$ , and  $R_{\text{CNT-Cu}}$  and the thermal diffusivity of each CNT array can be estimated.

When the thermal diffusion length in the gas is much less than the radius of the PA cell, the PA signal is independent of the energy distribution of the incident laser beam; therefore, a one-dimensional model of the PA effect is adequate.<sup>36</sup> The transient temperature field in the multilayer sample and gas can be derived by solving a set of one-dimensional heat conduction equations, and the transient temperature in the gas is related to the pressure, which is measured experimentally. Because the transient temperature in the gas is related to the thermal properties of the sample, measuring the pressure allows determination of the thermal quantities—in this work, the thermal interface resistance and thermal diffusivity. Details of the derivation have been described by Hu *et al.*<sup>23</sup> The solution of the complex temperature distribution  $\theta_{N+1}$  in the gas can be expressed as

$$\theta_{N+1} = (1 - \rho)B_{N+1}e^{-\sigma_{N+1}x}e^{j\omega t}, \quad (1)$$

where

$$B_{N+1} = - \frac{[0 \ 1] \sum_{m=0}^N \left( \prod_{i=0}^{m-1} U_i \right) V_m \begin{bmatrix} E_m \\ E_{m+1} \end{bmatrix}}{[0 \ 1] \left( \prod_{i=0}^N U_i \right) \begin{bmatrix} 0 \\ 1 \end{bmatrix}}, \quad (2)$$

$$U_i = \frac{1}{2} \begin{bmatrix} u_{11,i} & u_{12,i} \\ u_{21,i} & u_{22,i} \end{bmatrix}, \quad V_i = \frac{1}{2} \begin{bmatrix} v_{11,i} & v_{12,i} \\ v_{21,i} & v_{22,i} \end{bmatrix}, \quad (3a)$$

$$u_{1n,i} = (1 \pm k_{i+1} \sigma_{i+1} / k_i \sigma_i \mp k_{i+1} \times \sigma_{i+1} R_{i,i+1}) \times \exp(\mp \sigma_{i+1} l_{i+1}), \quad n = 1, 2, \quad (3b)$$

$$u_{2n,i} = (1 \mp k_{i+1} \sigma_{i+1} / k_i \sigma_i \mp k_{i+1} \times \sigma_{i+1} R_{i,i+1}) \times \exp(\mp \sigma_{i+1} l_{i+1}), \quad n = 1, 2, \quad (3c)$$

$$v_{n1,i} = 1 \pm \beta_i / \sigma_i, \quad n = 1, 2, \quad (3d)$$

$$v_{n2,i} = (-1 \mp k_{i+1} \beta_{i+1} / k_i \sigma_i + k_{i+1} \times \beta_{i+1} R_{i,i+1}) \times \exp(-\beta_{i+1} l_{i+1}), \quad n = 1, 2, \quad (3e)$$

$$E_m = \frac{G_m}{\beta_m^2 - \sigma_m^2}, \quad (4a)$$

$$G_m = \begin{cases} \frac{\beta_m I_0}{2k_m} e^{-\sum_{i=m+1}^N \beta_i l_i} & \text{for } m < N \\ \frac{\beta_m I_0}{2k_m} & \text{for } m = N \\ 0 & \text{for } m = N + 1. \end{cases} \quad (4b)$$

The  $x$  coordinate originates from the surface of the sample and points outward. In the above equations,  $\sigma_i = (1+j)a_i$  with  $j = \sqrt{-1}$  and  $a_i = \sqrt{\pi f l} \alpha_i$ , where  $\alpha_i$  is the thermal diffusivity of layer  $i$ ,  $f$  is the modulation frequency,  $k_i$  is the thermal conductivity of layer  $i$ ,  $\rho$  is the surface reflectivity of the sample,  $\beta_i$  is the optical absorption coefficient of layer  $i$ , and  $R_{i,i+1}$  is the thermal interface resistance between layers  $i$  and  $i+1$ . In the calculation,  $l_{N+1}$  is taken as 0, and  $\prod_{k=m}^{m-1} U_k$  is taken as the  $2 \times 2$  identity matrix, where  $m$  is any integer between 0 and  $N+1$ .

The temperature in the gas layer is related to the phase shift and amplitude of the PA signal. According to the theory of Hu *et al.*,<sup>23</sup> the phase shift of the PA signal is  $\text{Arg}(B_{N+1}) - \pi/4$  and the amplitude of the PA signal is  $\text{Abs}[(1-\rho)B_{N+1}P_0/\sqrt{2}l_{N+1}a_{N+1}T_0]$ , where  $P_0$  and  $T_0$  are the ambient pressure and temperature, respectively.

## 2. Experimental methods

A schematic of the experimental setup is shown in Fig. 4. A fiber laser operating at a wavelength of  $1.1 \mu\text{m}$  is used as the heating source. Laser power is sinusoidally modulated by an acoustic-optical modulator (AOM) driven by a function generator. For this study, the modulation frequency ranges from 300 to 750 Hz. The output power of the laser is approximately 350 mW in the modulation mode. After being reflected and focused, the laser beam is directed onto the sample mounted at the bottom of the PA cell. The PA cell is

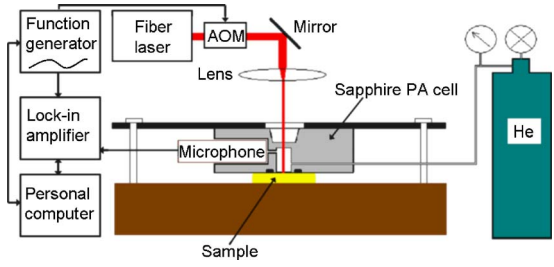


FIG. 4. (Color online) Schematic diagram of the PA apparatus.

pressurized by flowing compressed He as shown in Fig. 4, thus providing a uniform average pressure on the sample surface. The PA cell pressure is adjusted using a flow controller and is measured by a gauge attached to the flow line. The test pressures are chosen to span a range of pressures commonly applied to promote contact between a heat sink and a processor chip. A microphone, which is built into the PA cell, senses the acoustic signal and transfers it to a lock-in amplifier, where the amplitude and phase of the acoustic signal are measured. A personal computer, which is connected to the GPIB interface of the lock-in amplifier and function generator, is used for data acquisition and control of the experiment.

The PA cell in this experiment is cylindrical and made of sapphire. Sapphire has low reflectance and high transmittance for the laser wavelength used; therefore, most of the laser energy reflected from the sample surface transmits out of the cell. The cell is designed to have an axial bore of 4 mm diameter and 7 mm depth. The side of the bore facing the laser beam has a polished window and the other side is sealed by the sample with an o ring through the application of mechanical clamping. The microphone is mounted near the inside wall of the cell for maximum signal strength.

For the one-sided CNT interface, Ag foil ( $R_a = 0.06 \mu\text{m}$  and  $R_z = 0.4 \mu\text{m}$ , calculated according to Ref. 30) forms the top of the sample, while for the two-sided CNT interface the side of the Cu sheet not coated by the CNT array is the effective top of the sample. The sample structures are shown above in Fig. 3. To prepare the samples for PA measurements, an 80 nm top layer of Ti was deposited by electron beam deposition, thus allowing for the Ti film to absorb the same amount of laser energy as the Ti film on the reference sample (see below) during measurements. The Ag foil [hard, Premion® 99.998% (metals basis); Alfa Aesar, Inc.] was  $25 \mu\text{m}$  thick and the Cu sheet (Puratronic® 99.9999% (metals basis); Alfa Aesar, Inc.) was  $50 \mu\text{m}$  thick to allow for high sensitivity to the total interface resistance of the one- and two-sided CNT interfaces, respectively. The Si wafers (double-side polished and  $\langle 100 \rangle$  orientation; Universitywafer.com) were  $565 \mu\text{m}$  thick to ensure that the layer is thermally thick. Sensitivity calculations, performed by varying the magnitude of the total CNT interface resistance in the PA model at different heating frequencies, are plotted in Fig. 5 to illustrate the upper and lower bounds of interface resistance for the sample configurations in this work. The one-sided CNT interface sample has upper and lower measurement limits of  $\sim 100$  and  $0.1 \text{ mm}^2 \text{ K/W}$ , respectively. The two-sided CNT interface sample has upper and lower measure-

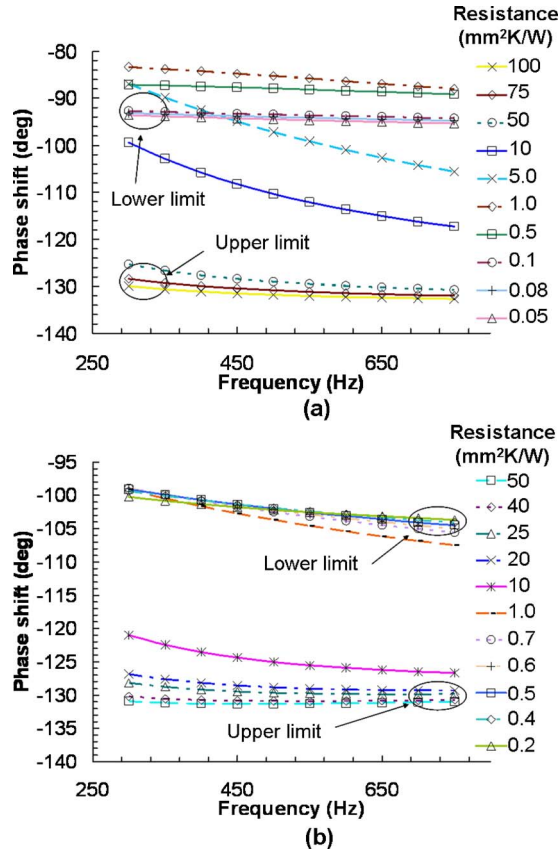


FIG. 5. (Color online) Sensitivity calculations performed by varying the magnitude of the total CNT interface resistance in the PA model and calculating a theoretical phase shift at different heating frequencies. The limits are identified as the resistances at which additional changes in resistance alter the calculated phase shift little such that further changes fall within experimental uncertainty. (a) Sensitivity for the one-sided CNT sample structure. Upper and lower measurement limits are  $\sim 100$  and  $\sim 0.1$   $\text{mm}^2 \text{K/W}$ , respectively. (b) Sensitivity for the two-sided CNT sample structure. Upper and lower measurement limits are  $\sim 35$  and  $\sim 0.4$   $\text{mm}^2 \text{K/W}$ , respectively.

ment limits of  $\sim 35$  and  $0.4$   $\text{mm}^2 \text{K/W}$ , respectively. The use of the hard,  $25$   $\mu\text{m}$  thick Ag foil in the one-sided CNT sample instead of the  $50$   $\mu\text{m}$  thick Cu sheet allows for greater measurement sensitivity. Cu sheets less than  $50$   $\mu\text{m}$  thick can improve measurement sensitivity as well; however, reduction in interface resistance resulting from the sheet's surface conformability (deformation between asperities) must be carefully considered in such a case. In general, the range of measurable resistances expands as the ratio of the thermal penetration depth to thickness increases for the top substrate (Ag and Cu in this work). The upper measurement limit results when the sample's effective thermal penetration depth is insufficient for allowing heat to pass through the interface and into the Si substrate; in this limit the interface is thermally thick. The lower measurement limit results when the sample's effective thermal penetration depth is much larger than the "resistive thickness" of the interface; in this limit the interface is thermally thin. For the frequency range and sample configurations of this study, a 1D heat diffusion analysis is applicable because the largest in-plane thermal diffusion lengths in the layered one-sided CNT sample,  $1/a_{\text{Ag}} = 0.43$  mm, and two-sided CNT sample,  $1/a_{\text{Cu}} = 0.35$  mm, are much less than the laser beam size (approximately  $1 \times 2$   $\text{mm}^2$ ).<sup>37</sup>

A reference or calibration sample is required for PA measurements in order to characterize signal delay due to the time needed for the acoustic wave to travel from the sample surface to the microphone and to account for possible acoustic resonance in the cell (resonance was not experienced for the cell in the frequency range of this study). A  $565$   $\mu\text{m}$  thick Si wafer with a top of  $80$  nm layer of Ti, deposited by electron beam deposition, was used as the reference sample (for uniformity, Ti was deposited on the reference and test samples at the same time). The reference was tested with the PA cell pressurized at different levels, including the pressure levels at which the samples were tested. According to PA theory, phase shift is independent of cell pressure, while amplitude is proportional to cell pressure. However, the signal delay may be pressure dependent for both phase shift and amplitude. The composition of the cell gas can change the nature of the cell signal delay as well. Air,  $\text{N}_2$ , and He were observed to cause different signal delay responses. Of these gases, He produced the highest signal to noise ratio, which is expected because the thermal conductivity of He is approximately an order of magnitude higher than that of air or  $\text{N}_2$ . He was therefore used as the cell gas for this work. The thermal diffusion length in the He filled PA cell,  $1/a_{\text{He}} = 0.46$  mm (at atmospheric pressure), is much less than the PA cell radius ( $4$  mm) which supports the assumptions of the PA model.<sup>36</sup>

The phase-shift signal is used in this work instead of the amplitude because it is more stable in the current experimental setup. Calibration was performed at each test pressure to account for pressure-dependent signal delay effects. The true phase shift of the sample,  $\phi$ , is calculated as  $\phi = \phi' - \phi'_{\text{Si,reference}} - 90$ , where  $\phi'$  is the measured phase shift for the CNT interface test sample and  $\phi'_{\text{Si,reference}}$  is the measured phase shift for the Si reference sample. Calibration was also performed before and after each measurement to account for any drift in the laser signal. At each frequency, the signal was first allowed to stabilize and then data were recorded every  $8$  s. The phase-shift data were averaged every  $5$  min and stored when the variation in average phase shift over the  $5$  min time span was less than  $0.2^\circ$  or after  $30$  min of collection.

### 3. Regression analysis and measurement uncertainty

The phase shift of the PA signal is  $\text{Arg}(B_{N+1}) - \pi/4$ , where  $B_{N+1}$  is a function of the densities, thermal conductivities, specific heats, thicknesses, optical absorption coefficients, and interface resistances in the multilayered sample, as shown in Eqs. (2)–(4) above. The known parameters in  $B_{N+1}$  are thermal properties that have been well characterized by other measurement techniques and are well documented in the literature.<sup>35,38</sup> The unknown parameters in  $B_{N+1}$  are determined by fitting the PA model to the experimentally measured phase-shift data. However, in order to determine an appropriate fitting procedure, the functional relationships among the PA model and the unknown parameters should be understood, and the relationship between unknown parameters and/or group of parameters (identifiability) should be analyzed.<sup>39</sup>

If only one parameter is unknown, as in estimating the total CNT interface resistance [Figs. 3(a) and 3(c)], the regression analysis is greatly simplified. Furthermore, when estimating the total CNT interface resistance,  $R_{\text{Si-Ag}}$  or  $R_{\text{Si-Cu}}$ , the model is linear with respect to the unknown parameter and guarantees a unique data fit. For this case, a basic least-squares fitting algorithm was used in which the square of the difference between the measured and theoretical signals calculated using trial unknown values was adjusted iteratively until a convergence criterion is satisfied ( $\sqrt{\sum_{n=1}^q [\phi_{\text{measured}} - \phi_{\text{theoretical}}]^2} / q < 0.1^\circ$ , for  $q$  tested laser frequencies).

The component resistances of the CNT interfaces are substantially more difficult to estimate with the PA model [Fig. 3(b) and 3(d)] due to numerous unknown parameters, nonlinear parameter relations, and identifiability limitations.<sup>39</sup> The fitting parameters used in this case include CNT array interface resistances, CNT array thermal diffusivity(ies), CNT array thermal conductivity(ies), and CNT array thickness(es). Additional data points, such that the number of measured signal-versus-frequency data points is at least equal to the number of unknown parameters, are required for the fitting of multiple parameters. The least-squares “best” fit for this nonlinear regression can have multiple solutions. However, it was found that, because the interface resistances dominate the thermal response on different time scales (or at different heating frequencies), the relatively wide frequency range used for the data fit allows for the interface resistances to be estimated with a high degree of identifiability. It was also found that the thermal response is insensitive to the low intrinsic thermal resistance of the CNT array(s) ( $l_{\text{CNT array}}/k_{\text{CNT array}}$ ), which is expected due to the high thermal conductivity of CNTs and the high density of the CNT arrays in this study, and consequently, the results are insensitive to the thermal conductivity and the thickness of the CNT array(s). Therefore, the only parameters that can be estimated include the thermal interface resistances and the thermal diffusivity(ies). To account for nonlinear parameter behavior, the least-squares algorithm is altered to perform a comprehensive parameter search<sup>39</sup> in the region where the sum of the squares is minimized while the unknown parameters are near their expected values. This technique requires the use of trial unknown values that are approximated based on literature data and simple models. For each case, it is possible for the least-squares algorithm to diverge if the experimental data are erroneous (i.e., not representative of the physics of the sample). When the regression is nonlinear, the accuracy of the values obtained from the least-squares fit depends on how much the unknown parameters can be changed or “pushed” from their best fit value while the minimized sum of squares changes little (i.e., the confidence interval).<sup>39,40</sup>

Experimental uncertainty is dominated by the uncertainty in the reference sample’s phase-shift signal ( $\pm 1.0^\circ$ ). The CNT interfaces exhibit a higher total resistance than the Si reference sample (which does not contain an interface), and as a consequence produce a stronger and more stable signal ( $\pm 0.2^\circ$ ). The effects of uncertainties associated with “known” material properties used in the PA model and un-

certainty associated with laser energy drift on the measured thermal properties were negligible in comparison to the effect of phase-shift uncertainty. The uncertainty in the estimated thermal properties is determined by finding the range of property values that yield the phase-shift values within their experimental uncertainty range. For the CNT interface samples, the resistance at the interfaces dominates the thermal response; therefore, the thermal diffusivity of each CNT array is more sensitive to small changes in the measured phase-shift signal. Consequently, the resulting thermal diffusivities exhibit greater uncertainty that increases as the measured interface resistance increases. Uncertainties in the resolved CNT interface resistances and the CNT arrays’ thermal diffusivity are also affected by the confidence intervals that result from nonlinear regression. However, these confidence intervals are small, having negligible effect on the total experimental uncertainty.

### III. RESULTS AND DISCUSSION

Using the PA technique, the thermal resistance of a one-sided CNT interface (Si-CNT-Ag) has been measured at 0.241 MPa and the thermal resistance of a two-sided CNT interface (Si-CNT-CNT-Cu) has been measured as a function of pressure. The PA technique has also been used to measure the component resistances of the CNT interfaces and the thermal diffusivities of the CNT arrays. All CNT interface measurements were performed at room temperature. After testing, the interfaces were separated and the CNT coverage on the Cu and Si substrates was observed visually to match the pretest condition. We believe that this resiliency is the result of the strong anchoring of the arrays to their substrates enabled by the trilayer catalyst. Figure 6 illustrates the fitted phase-shift results at 0.241 MPa for the CNT interface samples. Fitting lines that correspond to the  $\pm 1.0^\circ$  experimental uncertainty are also shown in Fig. 6. To establish a benchmark for the accuracy of the PA technique, a commercial TIM (Shin-Etsu  $25 \times 25 \text{ mm}^2$  thermal pad; Shin-Etsu Chemical Co., Ltd.) interface (Si-PCM-Cu) was tested. The TIM changes phase at  $48^\circ \text{C}$  and has a reported resistance of  $22 \text{ mm}^2 \text{ K/W}$  for a  $50 \mu\text{m}$  thick layer. A resistance of  $20 \text{ mm}^2 \text{ K/W}$  was measured with the PA technique for an approximate interface temperature of  $55^\circ \text{C}$  and pressure of 0.138 MPa, in good agreement with the manufacturer’s published value.

One-sided CNT interface results are summarized in Table I and two-sided CNT interface results are illustrated in Fig. 7 and summarized in Table II. The resistances at CNT-substrate interfaces (and the CNT-CNT interface for the two-sided interface) and the intrinsic conductive resistance of the CNT arrays are grouped into the measured total interface resistances  $R_{\text{Si-Ag}}$  and  $R_{\text{Si-Cu}}$ . This lumping approach has no effect on the measured results because during each measurement the laser energy penetrates deep enough to completely pass through  $R_{\text{Si-Ag}}$  and  $R_{\text{Si-Cu}}$  and into the Si substrate.

At a pressure of 0.241 MPa the one-sided CNT interface produces a thermal resistance of approximately  $16 \text{ mm}^2 \text{ K/W}$ . This photoacoustically measured resistance compares well with one-sided CNT interface results reported

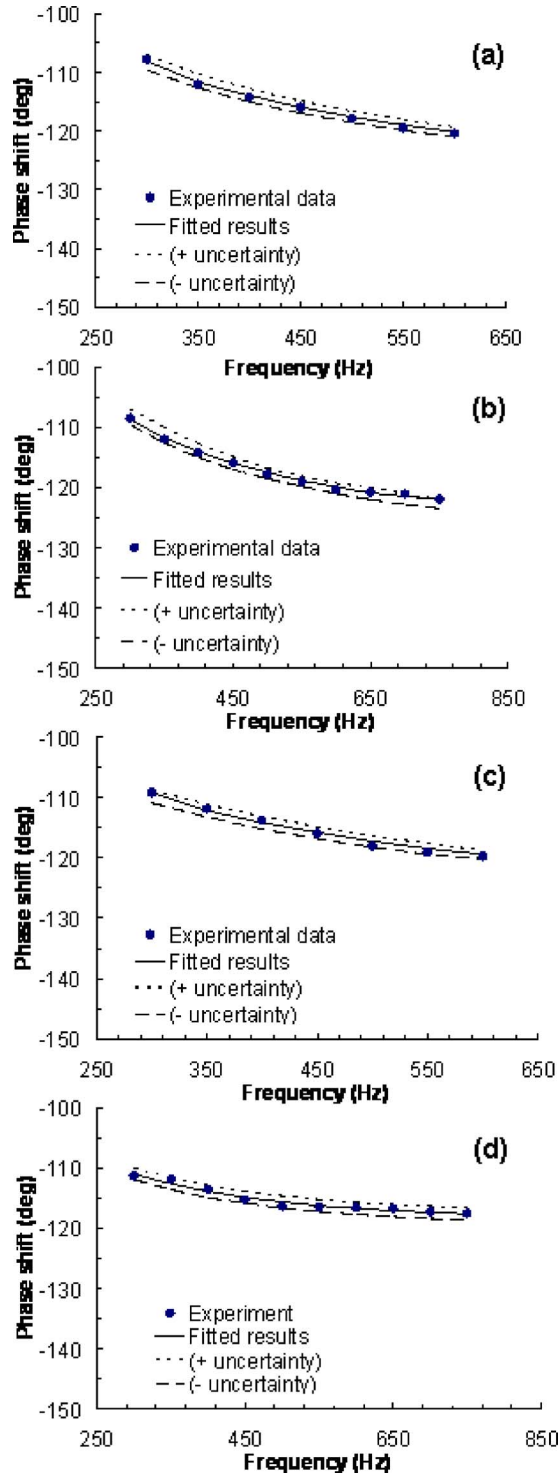


FIG. 6. (Color online) Phase shift as a function of modulation frequency for CNT interfaces with an applied contact pressure of 0.241 MPa. The mean-square deviation of all fits is approximately  $0.3^\circ$  in phase shift. (a) Lumped one-sided interface fitting results. (b) Resolved one-sided interface fitting results. (c) Lumped two-sided interface fitting results. (d) Resolved two-sided interface fitting results. The two-sided fitting data are typical of measurements at each pressure.

previously using a steady state, 1D reference bar measurement technique.<sup>13</sup> The resistances at the CNT-substrate interfaces,  $R_{\text{Si-CNT}}$  and  $R_{\text{CNT-Ag}}$ , are approximately 2 and 14  $\text{mm}^2 \text{K/W}$ , respectively, and it is clear that the resistance between the free CNT array tips and their opposing substrate

TABLE I. One-sided CNT interface results.

Fitted parameters	Measured values at 0.241 MPa
$R_{\text{Si-CNT}}$ ( $\text{mm}^2 \text{K/W}$ )	$1.7 \pm 1.0$
$R_{\text{CNT-Ag}}$ ( $\text{mm}^2 \text{K/W}$ )	$14.0 \pm 0.9$
$R_{\text{total}}(R_{\text{Si-Ag}})$ ( $\text{mm}^2 \text{K/W}$ ) <sup>a</sup>	$15.8 \pm 0.9$
$\alpha_{\text{CNTs-on-Si}}$ ( $\text{m}^2/\text{s}$ )	$(0.4-2.8) \times 10^{-4}$

<sup>a</sup>Obtained from data fit where the CNT arrays are not considered as a layer in the PA model.

( $R_{\text{CNT-Ag}}$ ) dominates the overall thermal resistance. A similar characteristic for one-sided CNT interfaces was reported in a previous study as well.<sup>17</sup> A thermal diffusivity in the range of  $(0.4-2.8) \times 10^{-4} \text{ m}^2/\text{s}$  is measured for the CNT array on the Si wafer in the one-sided CNT interface sample.

At moderate pressures of 0.172–0.379 MPa, the two-sided CNT interface produces stable and low resistances near 4  $\text{mm}^2 \text{K/W}$ . For comparison, resistance values of a two-sided CNT interface measured with a reference bar method<sup>15</sup> are also included in Fig. 7. The results demonstrate that the PA results are similar to the reference bar results and fall well within the latter's uncertainty range. The pressure dependent, two-sided CNT interface results validate a prior postulate<sup>15</sup> that data scatter in the resistance-pressure characteristics of the reference bar measurements is due to the large uncertainty associated with the method. The resolved thermal resistances of the two-sided CNT interface,  $R_{\text{Si-CNT}}$ ,  $R_{\text{CNT-CNT}}$ , and  $R_{\text{CNT-Cu}}$ , are approximately 1, 2, and 1  $\text{mm}^2 \text{K/W}$ , respectively. These resistances are stable in the tested pressure range and the maximum resistance of the two-sided CNT interface is always the resistance at the CNT-CNT interface. The range of thermal diffusivity measured for the CNT arrays in the two-sided interface are summarized in Table II.

The thermal performance revealed by the PA measurement of the one-sided CNT interface can be attributed to the increase in real contact area enabled by the high density of CNT to surface contact spots. The thermal performance revealed by the PA measurements of the two-sided CNT interface can be attributed to an even larger increase in real contact area. In this case, we postulate that the contact area between the two arrays is maximized during the initial load-

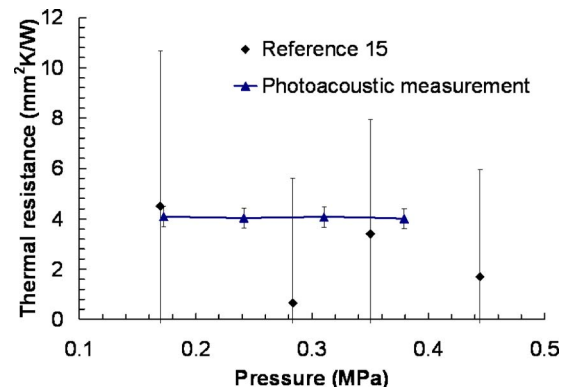


FIG. 7. (Color online) Thermal resistance as a function of pressure for a two-sided CNT interface ( $R_{\text{Si-CNT-CNT-Cu}}$ ) measured with the PA method and the 1D reference bar method of Ref. 15.

TABLE II. Two-sided CNT interface results.

Fitted parameters	Measured values at 0.172 MPa	Measured values at 0.241 MPa
$R_{\text{Si-CNT}}$ ( $\text{mm}^2 \text{K/W}$ )	$0.8 \pm 0.5$	$0.8 \pm 0.5$
$R_{\text{CNT-CNT}}$ ( $\text{mm}^2 \text{K/W}$ )	$2.1 \pm 0.4$	$2.1 \pm 0.4$
$R_{\text{CNT-Cu}}$ ( $\text{mm}^2 \text{K/W}$ )	$1.0 \pm 0.5$	$0.9 \pm 0.5$
$R_{\text{total}}(R_{\text{Si-Cu}})$ ( $\text{mm}^2 \text{K/W}$ ) <sup>a</sup>	$4.1 \pm 0.4$	$4.0 \pm 0.4$
$\alpha_{\text{CNTs-on-Si}}$ ( $\text{m}^2/\text{s}$ )	$(0.8-3.2) \times 10^{-4}$	$(2.3-6.5) \times 10^{-4}$
$\alpha_{\text{CNTs-on-Cu}}$ ( $\text{m}^2/\text{s}$ )	$(0.6-2.1) \times 10^{-4}$	$(1.4-4.3) \times 10^{-4}$

<sup>a</sup>Obtained from data fit where the CNT arrays are not considered as a layer in the PA model.

ing procedure, so that further increases in pressure do not cause a significant increase in array-to-array CNT penetration. This postulate is validated by the approximately constant value of  $R_{\text{CNT-CNT}}$  in the tested pressure range. Compared to the resistances of a bare Si-Cu interface<sup>14</sup> and a one-sided CNT interface (Si-CNT-Cu),<sup>14</sup> which range from 105 to 196 and 20–31  $\text{mm}^2 \text{K/W}$ , respectively, a two-sided CNT interface produces much lower thermal contact resistance. It is important to note that, as a dry interface, the two-sided CNT interface performs comparable to, if not better than, a soldered interface<sup>21</sup> and a phase change metallic alloy (PCMA) filled interface.<sup>41</sup>

The uncertainty in PA measurements of the total interface resistances  $R_{\text{Si-Ag}}$  and  $R_{\text{Si-Cu}}$  is less than  $\pm 1 \text{ mm}^2 \text{K/W}$ , which is significantly lower than the steady state, 1D reference bar method's uncertainty. Considering the agreement of the results from two different measurement techniques and between the measured commercial TIM resistance and the manufacturer's published value, the present work suggests that the PA method is a reliable experimental method for the precise measurement of thermal interface resistance.

#### IV. CONCLUSION

Well anchored and vertically oriented CNT arrays have been fabricated on Si wafers and Cu sheets by direct PECVD synthesis with a trilayer catalyst configuration. These two CNT-coated samples form a two-sided CNT interface and a CNT-coated Si wafer and bare Ag foil form a one-sided CNT interface. The thermal contact conductance enhancement of the two interfaces has been experimentally measured using a PA technique. The resistance of the one-sided CNT interface was measured to be approximately 16  $\text{mm}^2 \text{K/W}$  at moderate pressure and the resistances of the two-sided CNT interface were measured to be approximately 4  $\text{mm}^2 \text{K/W}$  with little pressure dependence. The results are consistent with those of previous steady state, 1D reference bar measurements of a one-sided CNT interface<sup>13</sup> and two-sided CNT interface,<sup>15</sup> but with a much narrower uncertainty range. PA measurements also revealed that the local interface resistance between the free CNT array tips and their opposing substrate, approximately 14  $\text{mm}^2 \text{K/W}$ , dominates the thermal resistance of the one-sided CNT interface, and the interface resistance between the two opposing CNT arrays, approximately 2  $\text{mm}^2 \text{K/W}$ , is the largest local resistance of the two-sided CNT interface. Using the PA technique, the component resistances of the CNT interfaces have been measured with rea-

sonable confidence, and the thermal interface resistance between two mating CNT arrays ( $R_{\text{CNT-CNT}}$ ) has been measured experimentally.

This study reveals that the PA technique can be a reliable and precise experimental method for the measurement of thermal interface resistance of separable (nonbonded) interfaces. Also, the PA technique developed in this work allows for interface resistance to be measured as a function of pressure by simply pressurizing the acoustic chamber. However, when using the PA technique with a pressurized acoustic chamber and sample, calibration may be needed to account for variations in signal delay with pressure and cell gas composition.

In this study the catalyst metal used for all CNT growths was Ni. The thermal conductance of two-sided CNT interfaces with CNTs grown from other catalysts remains to be studied. The effects of different synthesis conditions on the thermal conductance of CNT interfaces also remain an area for further study. The effects of substrate surface roughness on the thermal performance of CNT interfaces along with the performance of CNT interfaces created by using substrates of different materials should be studied as well. The PA measurements in this study were performed at room temperature, and CNT conductance in the high and low temperature regimes warrants investigation. Characterization of the thermal performance of CNT interfaces while an electrical current flows through the interface is also possible using the PA technique. The component resistance measurements in this study produced the largest error in terms of percentage. Resolving these resistances with even greater precision is an issue that necessitates further study. The physics that governs the thermal transport in CNT array interfaces is complex. The measurement of CNT-substrate and CNT-CNT interface resistances for isolated CNTs (as apposed to arrays) would contribute significantly to the understanding of this transport. Developing a model that can adequately predict the thermal transport in CNT array interfaces is a needed focus for future research as well.

#### ACKNOWLEDGMENTS

The authors gratefully acknowledge funding from the NASA Institute for Nanoelectronics and Computing (INaC), the National Science Foundation (CTS-0646015), and the Cooling Technologies Research Center at Purdue University in support of this work. Baratunde Cola also acknowledges support from the Purdue University Graduate Ph.D. Fellowship and the Intel Foundation Ph.D. Fellowship. Hanping Hu also acknowledges support from NSFC (Grant No. 50476024).

<sup>1</sup>S. Iijima, *Nature (London)* **354**, 56 (1991).

<sup>2</sup>M. Terrones, *Annu. Rev. Mater. Res.* **33**, 419 (2003).

<sup>3</sup>S. Berber, Y. K. Kwon, and D. Tomanek, *Phys. Rev. Lett.* **84**, 4613 (2000).

<sup>4</sup>J. W. Che, T. Cagin, and W. A. Goddard, *Nanotechnology* **11**, 65 (2000).

<sup>5</sup>P. Kim, L. Shi, A. Majumdar, and P. L. McEuen, *Phys. Rev. Lett.* **87**, 215502 (2001).

<sup>6</sup>S. Maruyama, *Microscale Thermophys. Eng.* **7**, 41 (2003).

<sup>7</sup>M. M. J. Treacy, T. W. Ebbesen, and J. M. Gibson, *Nature (London)* **381**, 678 (1996).

<sup>8</sup>K. Enomoto, S. Kitakata, T. Yasuhara, T. Kuzumaki, Y. Mitsuda, and N. Ohtake, *Appl. Phys. Lett.* **88**, 153115 (2006).

- <sup>9</sup>H. F. Chuang, S. M. Cooper, M. Meyyappan, and B. A. Cruden, *J. Nanosci. Nanotechnol.* **4**, 964 (2004).
- <sup>10</sup>X. Hu, A. A. Padilla, J. Xu, T. S. Fisher, and K. E. Goodson, *J. Heat Transfer* **128**, 1109 (2006).
- <sup>11</sup>Q. Ngo, B. A. Gurden, A. M. Cassell, M. D. Walker, Q. Ye, J. E. Koehne, M. Meyyappan, J. Li, and C. Y. Yang, *Nano Lett.* **4**, 2403 (2004).
- <sup>12</sup>J. L. Sample, K. J. Rebello, H. Saffarian, and R. Osiander, Proceedings of the Ninth Intersociety Conference on Thermal and Thermomechanical Phenomena in Electronic Systems, Las Vegas, Nevada, 2004 (unpublished), pp. 297–301.
- <sup>13</sup>J. Xu and T. S. Fisher, *IEEE Trans. Compon. Packag. Technol.* **29**, 261 (2006).
- <sup>14</sup>J. Xu and T. S. Fisher, *Int. J. Heat Mass Transfer* **49**, 1658 (2006).
- <sup>15</sup>J. Xu and T. S. Fisher, Proceedings of the 18th National and 7th ISHMT-ASME Heat and Mass Transfer Conference, IIT Guwahati, India, 2006 (unpublished), Paper No. HTC-2006-C336.
- <sup>16</sup>X. Wang, Z. Zhong, and J. Xu, *J. Appl. Phys.* **97**, 064302 (2005).
- <sup>17</sup>T. Tong, Y. Zhao, L. Delzeit, A. Kashani, A. Majumdar, and M. Meyyappan, Proceeding of the ASME International Mechanical Engineering Congress and Exposition, Orlando, Florida, 2005 (unpublished), Paper No. IMECE2005-81926.
- <sup>18</sup>M. Panzer, G. Zhang, D. Mann, X. Hu, E. Pop, H. Dai, and K. E. Goodson, Proceedings of the Itherm 2006, San Diego, California, 2006 (unpublished), pp. 1306–1313.
- <sup>19</sup>International Technology Roadmap for Semiconductors (ITRS), <http://www.itrs.net/Common/2005ITRS/Home2005.htm>.
- <sup>20</sup>T. Tong, Y. Zhao, L. Delzeit, A. Majumdar, and A. Kashani, Proceedings of the ASME Integrated Nanosystems, Pasadena, California, 2004 (unpublished), Paper No. NANO2004-46013.
- <sup>21</sup>D. D. L. Chung, *Appl. Therm. Eng.* **21**, 1593 (2001).
- <sup>22</sup>A. Rosencwaig and A. Gersho, *J. Appl. Phys.* **47**, 64 (1976).
- <sup>23</sup>H. Hu, X. Wang, and X. Xu, *J. Appl. Phys.* **86**, 3953 (1999).
- <sup>24</sup>A. Tam, *Rev. Mod. Phys.* **58**, 381 (1986).
- <sup>25</sup>A. Lachaine and P. Poulet, *Appl. Phys. Lett.* **45**, 953 (1984).
- <sup>26</sup>S. S. Raman, V. P. N. Nampoori, C. P. G. Vallabhan, G. Ambadas, and S. Sugunan, *Appl. Phys. Lett.* **67**, 2939 (1995).
- <sup>27</sup>M. Rohde, *Thin Solid Films* **238**, 199 (1994).
- <sup>28</sup>X. Wang, H. Hu, and X. Xu, *J. Heat Transfer* **123**, 138 (2001).
- <sup>29</sup>B. A. Cola, R. Karru, C. Cheng, X. Xu, and T. S. Fisher, *Proceedings of the Itherm, San Diego, California, 2006*, [IEEE Trans. Compon. Packag. Technol. (submitted)].
- <sup>30</sup>*Surface Texture (Surface Roughness, Waviness and Lay)* (American Society of Mechanical Engineers, New York, 2003).
- <sup>31</sup>M. R. Maschmann, P. B. Amama, A. Goyal, Z. Iqbal, R. Gat, and T. S. Fisher, *Carbon* **44**, 10 (2006).
- <sup>32</sup>M. Meyyappan, L. Delzeit, A. Cassell, and D. Hash, *Plasma Sources Sci. Technol.* **12**, 205 (2003).
- <sup>33</sup>M. Chhowalla, K. B. K. Teo, C. Ducati, N. L. Rupesinghe, G. A. J. Amaratunga, A. C. Ferrari, D. Roy, J. Robertson, and W. I. Milne, *J. Appl. Phys.* **90**, 5308 (2001).
- <sup>34</sup>K. Biljakovic, A. Smontara, D. Staresinic, D. Pajic, M. E. Kozlov, M. Hirabayashi, M. Tokumoto, and H. Ihara, *J. Phys.: Condens. Matter* **8**, L27 (1996).
- <sup>35</sup>F. P. Incropera and D. P. DeWitt, *Fundamentals of Heat and Mass Transfer* (Wiley, New York, 2002).
- <sup>36</sup>R. S. Quimby and W. M. Yen, *J. Appl. Phys.* **51**, 1252 (1979).
- <sup>37</sup>H. C. Chow, *J. Appl. Phys.* **51**, 4053 (1980).
- <sup>38</sup>E. D. Palik, *Handbook of Optical Constants of Solids* (Academic, San Diego, 1985).
- <sup>39</sup>J. V. Beck and K. J. Arnold, *Parameter Estimation in Engineering and Science* (Wiley, New York, 1977).
- <sup>40</sup>T. D. Bennett and Fengling Yu, *J. Appl. Phys.* **97**, 013520 (2005).
- <sup>41</sup>E. C. Samson, S. V. Machiroutu, J. Y. Chang, I. Santos, J. Hermerding, A. Dani, R. Prasher, and D. W. Song, *Intel Technol. J.* **9**, 75 (2005).